Bull. Soc. Photogr. Imag. Japan. (2019) Vol. 29 No. 2: 20–26

Original Paper

Desensitized Nuclear Emulsion Films for Measuring the Chemical Composition of Cosmic-ray Nuclei

Saya Yamamoto*, Shigeki Aoki***, Atsushi Iyono**, Keita Ozaki***, Satoshi Kodaira****, Misato Yabu***

Abstract: Highly sensitive nuclear emulsion films and high-speed imaging technology have been developed for recording tracks of minimum ionization particles such as cosmic-ray muons and electrons. The ionization energy of the heavy ions in cosmic rays is too high to identify the individual nuclear charges because the signal of pulse-height volume for tracks is saturated on this system. We have developed desensitized nuclear emulsion films by adding a rhodium compound ($Na_3RhCl_6 \cdot 5H_2O$). This modification reduces the film's sensitivity to heavy ions by 37%, resulting in better linearity between ionization energy and the signal of the tracks. The signals due to heavy ions were compared with the signals recorded on a CR-39 nuclear track-detector. The desensitized nuclear emulsion films successfully distinguished adjacent nuclear charges of heavy ions.

Key words: Nuclear emulsion film, Cosmic-ray nuclei, CR-39, Rhodium compound, Nuclear track detector

1. Introduction

Recent innovations in producing nuclear emulsion have enabled novel experiments in particle physics. Emulsion gels have been produced with various grain sizes and various types of silver-halide weight-content (in the emulsion) [1]. Films coated with these gels can record charged particle tracks with sub-micrometer spatial resolution[2] and diminish the prevalence of latent image specks under the highly humid environments[1] (refreshing process). The swelling process was also well operated to restore the original thickness of emulsion layer[3]. These processes are used to image neutrinos in the OPERA[4] and NINJA[5] experiments, search for MeV cosmic gamma rays in the GRAINE experiment[6, 7], and for muon tomographic imaging of volcanoes, blast furnaces and the pyramids at Giza[8]. Furthermore, these applications also depend on the high-speed track-recognition system that is used to analyze tracks recorded in nuclear emulsion films. The Hyper-Track Selector (HTS) instruments has increased the scanning speed for digitizing images of emulsion film to recognize track information without huge image data set. Owing to this development, nuclear emulsion films have been used in several experiments in which spatial resolution and angular resolution are required to be less than one micrometer and less than milliradians, respectively. In these high-performance track analyses, the read-out systems are adjusted to detect minimum ionized particles (MIP). Signals by high atomic-number (Z) particles like heavy nuclei would be saturated and such particles cannot be identified each other.

Emulsion technologies are used to detect cosmic gamma rays with new nuclear emulsion films in the GRAINE balloon flight experiments[6, 7]. In these experiments, the tracks of electron and positron pairs formed by gamma-ray conversion in the detector must be distinguished among the huge number of noise tracks. These films are very useful for recognizing the trajectories efficiently. Detection performance for cosmic-ray nuclei with these films is limited, however, because the HTS analyses are optimized for detecting MIP tracks like those left by electrons.

The majority, 99%, of cosmic-ray nuclei are composed of hydrogen and helium. Only one percent of cosmic-ray nuclei are heavier nuclei like C, N, O or Fe. These heavier species provide information about the origin, acceleration mechanism and propagation of cosmic-ray nuclei. The elemental abundance of cosmic-ray nuclei above Z = 30 can reveal the origin of the cosmic ray, which may include supernova explosions, rapid-process and slow-process neutron capture, neutron-star mergers[9], stellar nucleosynthesis or the chemical evolution of the galaxy. The emulsion films lifted up to the height of 40 km above sea level in the GRAINE experiment recorded cosmic-ray nuclei. Highly ionized particles such as high atomic number (Z) particle or low energy particle, however, are eliminated by the HTS algorithm during image analysis. To bring out the best ability of HTS system, we have decided to produce desensitized nuclear emulsion gels by controlling the chemical compounds added. The

Received 25th July 2019; Accepted 14th December 2019

*Graduate School of Science, Okayama University of Science, 1-1, Ridai-cho, Kita-ku, Okayama-shi, Okayama 700-0005, Japan
**Faculty of Science, Okayama University of Science, 1-1, Ridai-cho, Kita-ku, Okayama-shi, Okayama 700-0005, Japan
***Faculty of Human Development, Kobe University, 3-11, Tsurukabuto, Nada-ku, Kobe-shi, Hyogo 657-8501, Japan
****National Institute of Radiological Sciences, 4-9-1, Anagawa, Inage-ku, Chiba-shi, Chiba 263-8885, Japan

tracks made by heavy cosmic-ray nuclei in these desensitized films behave as if they are MIP tracks in HTS analysis.

To calibrate the extent to which various chemical compounds desensitize the nuclear emulsion gels, we performed the heavy-ion irradiation experiments with several nuclei. We also compared the HTS results against the etched pit size of solid-state track-detector of CR-39 whose sensitivity is lower than that of the original nuclear emulsion.

2. Methods and material

2.1 Automatic nuclear emulsion readout system

To obtain data about ion tracks such as positions, angles and ionization loss in nuclear emulsion film, microscopic measurements have to be taken after the films are developed with chemicals. Although this analysis was once done manually with a microscope and was consequently very time-consuming, the development of the HTS[2] allows us to obtain track data in extremely short times.

The HTS readout system has a very wide field of view and reaches a scanning speed of 4700 cm^2/h in recognizing single tracks. To utilize the HTS abilities for detecting highly ionized particles, these tracks must be made to resemble the tracks by MIPs. The pulse height volume (PHV) data output by HTS scanning can be used to identify nuclear species via the total amount of ionization energy loss along the tracks. The PHV signal by highly ionized particles such as relativistic heavy ions is saturated in typical high-sensitivity nuclear emulsion film because many knock-on electrons lay along them and the field of view (FoV) of HTS filled up with them. Delta-rays also make the PHV fluctuate because some delta-rays go out the FoV of HTS. The PHV in desensitized nuclear emulsion films are therefore utilized for measuring ionization losses along the tracks, similar to classical track-width measuring methods[11].

PHV values can be used to detect heavy ions with three modifications: (1) higher illumination in image analysis, (2) shorter chemical developing time or (3) desensitized nuclear emulsion film. The HTS's light intensity is limited by the uniformity of the wide FoV and changing the chemical development process might have unpredictable results. We therefore selected the third option for testing.

2.2 Desensitized nuclear emulsion films and solid-state track detector

We tested two types of nuclear emulsion gel with different silver-halide weight-content in the emulsion gel. This follows the difference of volume-occupancy by silver-halide in the gel. High-volume-occupancy gels have silver bromide crystals taking up approximately 55% of the gel's volume (abbreviated as H). Middle-volume-occupancy gels have silver bromide crystals taking up approximately 45% of the gel's volume (abbreviated as M).

To desensitize the nuclear emulsion film, sodium hexachlororhodate (III) 5-hydrate (rhodium compound, $Na_3\ RhCl_6\ \cdot 5H_2\ O$) was added when producing the nuclear emulsion gel or 2,3-bis (4-methoxyphenyl)-5-phenyltetrazolium chloride (tetrazolium compound, $C_{21}\ H_{19}\ ClN_4\ O_2$) was added to the nuclear emulsion gel before applying it on a film base. The sensitivity can be controlled by adjusting the total amount of each additive. We prepared three type of desensitized emulsion films for testing. We added rhodium compound into the no ripening samples to achieve a rhodium concentration of 2.5 μmol/Ag mol (abbreviated as NRHRhS in the following section) and 5.0 μmol/Ag mol (abbreviated as NRHRhL), respectively. The tetrazolium compound was added into the ripening sample at a concentration of 20 μmol/Ag mol (abbreviated as NRHTz). These samples are summarized in Table 1.

We applied a nuclear emulsion gel consisting mainly of silver bromide to both surfaces of a plastic film base to make samples of nuclear emulsion film. The thickness of the nuclear emulsion layer was designed to be 60 μm on both sides of the plastic films, whose thickness was 180 μm. Therefore, the total thickness of each nuclear emulsion film was nominally 300 μm. These emulsion films were prepared at Nagoya University in Japan[1), 7)].

CR-39 plate (Sun9 produced by Sunlux Co. ltd.) was deployed at the furthest downstream side of the chamber. CR-39 is a solid-state nuclear track detector that allows us to determine energy loss of beam by measuring the size of the pits formed on the detector due to incident ions.

3. Irradiation experiment of heavy ion beams

3.1 Irradiation experiment

To calibrate the sensitivities of the desensitized emulsion film samples, we irradiated each emulsion film with heavy ion beams of

Table 1 List of nuclear emulsion films used here with numbering and abbreviations.

Number	Abbreviation	Type of nuclear emulsion films	Additive
1	RM	Ripening and middle-volume occupancy	None
2	NRH	No ripening and high-volume occupancy	None
3	NRHTz	No ripening and high-volume occupancy	Tetrazolium compound 20 μ mol/Ag mol
4	NRHRhS	No ripening and high-volume occupancy	Rhodium compound 2.5 μ mol/Ag mol
5	NRHRhL	No ripening and high-volume occupancy	Rhodium compound 5.0 μ mol/Ag mol

Table 2 List of high-energy ion beams used here. Irradiation energy was 350 MeV per nucleon for each ion.

Irradiation particle	Electric charge	Irradiation energy [MeV/n]	Ionization energy loss [MeV cm^2g^{-1}]
Li	3	350	22
Be	4	350	40
B	5	350	62
C	6	350	90

lithium, beryllium, boron and carbon with energies of 350 MeV per nucleon. These tests were performed at HIMAC (Heavy Ion Medical Accelerator at Chiba) in National Institute of Radiological Sciences on October 26, 27 and 31 in 2017. The beam characteristics are summarized in Table 2.

For these tests, we constructed an emulsion chamber block with five types of emulsion films and a CR-39 plate, which is shown in Fig. 1. The exposed dimension of the chamber was 50 mm × 50 mm and its thickness was 85 mm. Four chambers shown in Fig. 1 were prepared for each ion beam exposure.

The direction and amount of irradiation applied in these tests are summarized in Table 3. We tilted the chambers toward the z direction of each beam shown in Fig. 1, at 0°, 20° and 40° and toward the y direction of each beam at 20°.

3.2 Processings of nuclear emulsion films and CR-39 plates

We developed the nuclear emulsion films[12] after the irradiation experiments. The NRHTz films were blacked out over the entire surface. The other emulsion films were developed without any errors. After developing, we scanned the nuclear emulsion films with HTS, after we swabbed them to remove silver deposits and swelled them. The swelling processes were carried out to restore the original thickness of nuclear emulsion layer by bathing in 20°C to 30°C water and 30% to 35% glycerin aqueous solution for the adequate duration.

As the films were swelled, black specks appeared in the sensitized

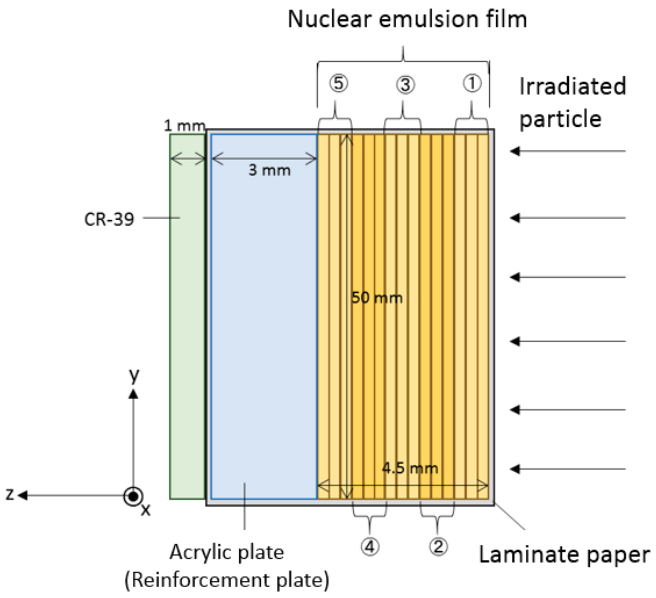

Fig. 1 Schematic structure of the chamber. Numbering of the nuclear emulsion films is summarized in Table 1.

Table 3 Beam direction and total amount of ions. These angles are given in degree unit in both x and y directions shown in Fig. 1

Direction (x degree, y degree)	Amount of irradiation (/25 cm^2)
(0, 20) for calibration	4×10^4
(0, 0)	8×10^4
(20, 0)	4×10^4
(40, 0)	4×10^4

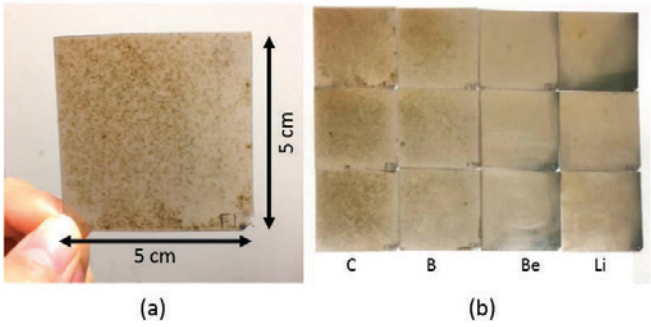

Fig. 2 (a) Photograph of a nuclear emulsion film (RM) in the carbon irradiated chamber, (b) Photographs of sets of three pieces with nuclear emulsion films (RM) irradiated with each ion. The scale of one film is 5 cm × 5 cm.

and middle-volume occupancy emulsion films, as shown in Fig. 2-a. As one can see in Fig. 2-b, black specks appeared most frequently in these three pieces of ripening emulsion film (abbreviated as RM) when exposed to carbon ions. The variations in the frequency of black specks caused by the four different ions in the same film are still not understood. The black specks are typically more than 100 μm in diameter. HTS ordinarily recognizes large size black objects as noise[2] by applying a low-pass-filtering algorithm. These large black specks were eliminated from the digitized track data, but fragments of these specks affected the estimation of the ionization energy described below.

We chemically etched the exposed CR-39 plates with 1 mm original thickness, in the 30 wt% aqueous sodium hydroxide solution at a temperature of 80°C for 60 minutes. The etched pit sizes along both major and minor axes have been measured by using HSP-1000 developed by Kodaira et al[13].

3.3 Emulsion Scanning

HTS recognized tracks in the following procedures; ① we binarized the image of each tomograph, ② we searched black pixel groups in each layer which were connected each other through 16 layers, ③ we considered the chain of black pixel group as a track and estimated three-dimensional information, such as position (x, y, z) etc., ④ we shifted the coordinate of each group as the line of pixel group through layers was perpendicular to the film, ⑤ we counted the number of pixels which were black in the 16 layers at each coordinate position of the pixel, ⑥ we defined the maximum value of pixel number in the group as PH, ⑦ we obtained the number of black pixels at the coordinate position of each pixel within the pixels whose number was greater than 9 in the 16 layers and summed up the number in the black group and ⑧ we defined this sum as PHV value for the track indicated by the black group. After all these pro-

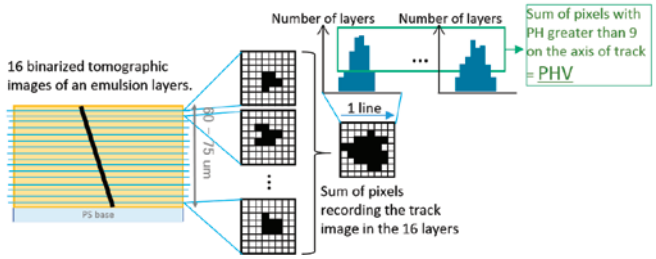

Fig. 3 Conceptual diagram of the algorithm to obtain PH (pulse height) and PHV (pulse height volume).

cedures, HTS returns data about three-dimensional positions (x, y, z) at the end of track touching the plastic film base, incident and orientation angles to the emulsion film, pulse height (PH) and PHV. HTS provides the horizontal coordinates (x, y) with an accuracy of 0.5 μm, the resolution along the optical axis (depth coordinate: z) became 2.1 μm[2]. The incident angle can be determined with an accuracy of 2.8 mrad by comparing the track positions on both sides of the plastic film base (180 μm). PHV is an indication of the size of ionization energy loss for MIP, gray track, black track and highly ionized particles. PHV indicates the degree of ionization loss per unit track length, which ranges from 0 to 1024 per emulsion layer. A schematic view of the HTS process is shown in Fig. 3.

4. Results

4.1 Analyses of PHV distribution

We have analyzed the PHV distributions of C, B, Be and Li ions at the beam energy of 350 MeV per nucleon in RM, NRHRhS, NRHRhL films except for NRHTz films which were blacked out. Those NRHTz films were preserved in a vacuum over the fifty hours between the irradiation experiments and development. Kuge et al.[8] reported that tetrazolium compound greatly increases the sensitivity of the nuclear emulsion film when it is stored in a vacuum. Fig. 4-a, -b and -c show the PHV distributions of each ion in RM, NRHRhS and NRHRhL films, where the obtained PHV data are summed values with both emulsion layers in the three films. In Fig. 4-a, the PHV values for each ion are distributed in the PHV range from 400 to 800. Though the PHV ranges of Li and those of the other higher-charged ions are separated, distributions of PHV for Be, B and C ions overlap and cannot be separated. So, in case of RM, we cannot distinguish what kind of ion forms the track. In case of NRHRhS emulsion films shown in Fig. 4-b, each PHV value for Li to C ions can be distinguished. The PHV distributions in the most desensitized nuclear emulsion film (NRHRhL) are shown in Fig. 4-c. PHV values are smaller than those of RM or NRHRhS and no PHV

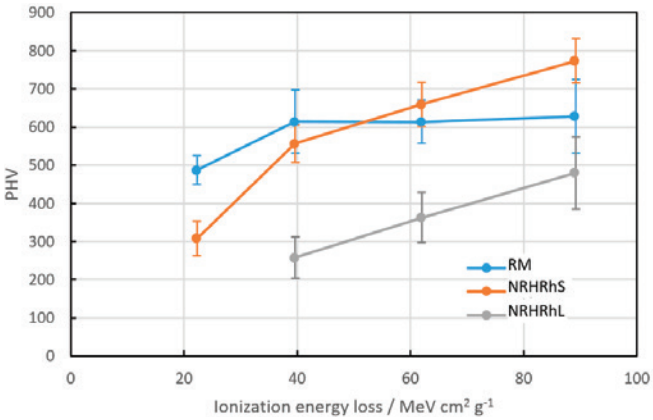

Fig. 5 Correlation of PHV with ionization energy loss. Blue, orange and gray dots represent types of nuclear emulsion films of RM, NRHRhS and NRHRhL, respectively.

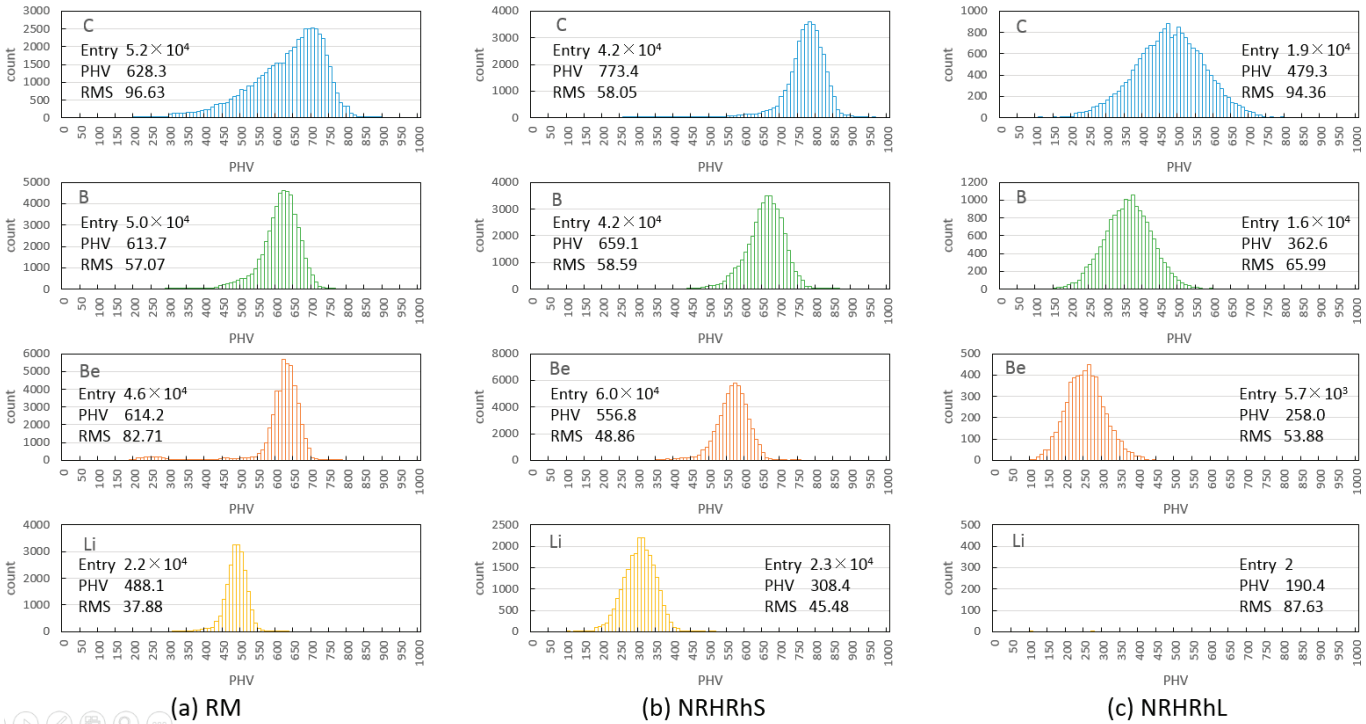

Fig. 4 Analyzed PHV distribution for each emulsion film and each ion.

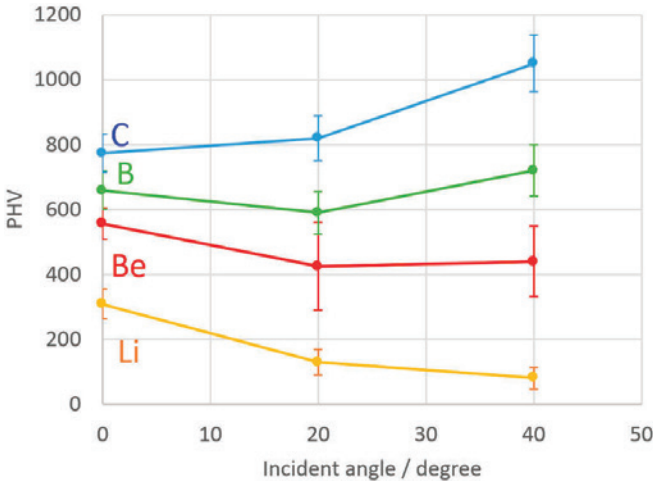

Fig. 6 Dependence of irradiation angle to the average of PHV at NRHRhS sample. Blue, green, red and yellow dots correspond to carbon, boron, beryllium and lithium ion beams, respectively.

signal corresponding to Li ions appeared. In this emulsions, Be, B and C ions were identified in the PHV range of 100 to 700. The separation ability between ion species is similar to that in the NRHRhS emulsions.

To compare the peak values of PHV for Li, Be, B and C ions with their ionization energy losses in the middle-volume occupancy emulsion film, we calculated these ionization energy losses by using Bete-Bloch formula[14], which are listed in the fourth column of Table 2. In Fig. 5, the peak positions of the PHVs for Li, Be, B and C ions obtained in Fig. 4 , were plotted as a function of ionization energy losses listed in Table 2.

The relationship between PHV and the incident angle of the ion beam has been discussed in several papers[15]. To determine how PHV depends on the incident angle, we exposed emulsion chambers at three different alignments to the beam line. The averaged PHV values in NRHRhS samples for each ion are plotted as a function of incident angles in Fig. 6. When the front side of the emulsion chamber is perpendicular to the beam line (0°), the PHV values are the same as those shown in Fig. 4-b. At the incident angle of 20°, the PHV decreased for B, Be and Li ions but not for the C ions. On the other hand, at 40° incident angle, the PHV values for Be, B and C ion except Li ion increased from those values at 20°.

4.2 Correlation of PHV and etched pit-size of solid-state track-detector (CR-39)

We deployed CR-39 solid-state track-detectors downstream of each emulsion chamber to calibrate the PHV values via comparison with the etched pit sizes along the minor axis. This test follows Kuge et al.'s calibration of comparing the OPERA film produced by Fuji film PHV and CR-39[16]. They reported the saturation of PHV.

The distributions of etched pit size along the minor axis for the ions hitting perpendicular to the beam line are shown in Fig. 7. These distributions were also fitted by Gaussian functions around their peak position. We obtained the averaged etched pit size from Be, B and C as 1.80±0.18, 2.03±0.16 and 2.37±0.14 μm, respectively. Li ions do not make any etched-pits and cannot be detected on CR-39. The second small peak of etched pit size in the C ions lay around 1.5 μm. This would come from the secondary fragments of C ions.

Finally, we compare the averaged PHV values with the minor axes of etched pit size for Be, B and C ions recorded on NRHRhS in Fig. 8-a and on NRHRhL in Fig. 8-b. The PHVs in both desensitized emulsion plates correlated to the etched pit sizes very well. NRHRhS gives slightly better linearity than NRHRhL does.

5. Discussion

To identify the charge of heavy ions, the ionization loss of each

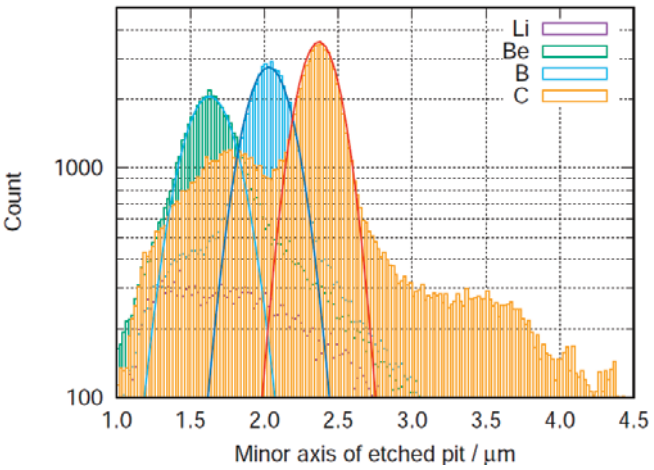

Fig. 7 Histogram of etched pit sizes at the minor axis recorded on CR-39 plate by each ion entered perpendicular to the plate. The etched pit sizes were measured using HSP-1000. Each color (purple, green, blue and red) of histograms corresponds to the irradiated ions of Li, Be, B and C, respectively. Gaussian-distribution fitting to each peak is also shown as colored lines of yellow, blue and red, respectively.

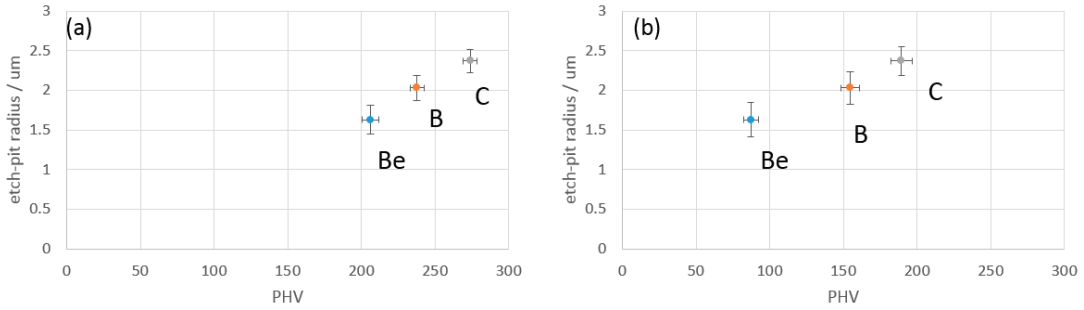

Fig. 8 Correlation of PHV at (a) NRHRhS and (b) NRHRhL with the etched pit size.

track in terms of PHV in the desensitized nuclear emulsion films was used. In case of NRHRhS, the peak values of PHV estimated from the distribution of PHV in Fig. 4 were well expressed as a linear function of the calculated values from Bete-Bloch ionization formula except for Li ions. In the RM films, PHV values for each ion were around 600. We cannot distinguish the ions from each other in this case. Therefore, in order to identify the charge of heavy ions with nuclear emulsion film and HTS system, the PHV values for the desensitized films are valuable to obtain the effective information. This mechanism is equivalent to traditional track width measurements made with photo-metrical methods[11]. Heavy ions typically produce a lot of knock-on electrons (delta-rays), with energies above 5 keV and the delta-ray range spectrum should be used to determin the Z^2/β^2 factors of ionization energy losses, where β is the speed of particle relative to the one of light, c. This is called the delta-ray count method. Delta-rays with energy less than 5 keV are partially effective in the formation of latent images along the track, which is referred as effective local ionization. But the delta-rays with energy from 5 keV to the maximum kinetic energy $\sim 2m_e c^2$ tend to be tied into knots by scattering and are therefore closely confined to the region of the trajectory of heavy ions. Therefore, these delta-rays would be cause PHV increase and finally be saturated in digital image analysis.

Furthermore, the HTS system accumulates binary pixel values in tomographic images along the track to determine track likelihoods and integrates all total pixel numbers above the threshold(PH $\geqq$ 9) to obtain the PHV of each track. The PHV for Be, B and C was saturated in the RM films because delta-rays of energy above 5 keV travel for several micro meter, overlap with each other and normally spill over the HTS window size (26 μm × 26 μm). On the other hand, the HTS system focuses on the analysis of single charged particles without higher-energy delta-rays to distinguish electrons, mesons and baryons produced by reactions of elemental particles, because those particles leave latent images via delta-rays of energy less than 5 keV. So we actively eliminate delta-rays from heavy ion tracks in order for HTS to recognize these tracks as being MIP or lower ionized particles. Therefore, we decided to desensitize nuclear emulsion films.

The desensitization of nuclear emulsion film suppresses the production of delta-rays. Consequently, by using PHV obtained from HTS, the sensitivities of NRHRhS film was reduced by 37% relative to the RM film and that of NRHRhL films was reduced by 54% relative to the NRHRhS film for a Li beam as shown in Fig. 5, when we regard the PHV value as a sensitivity of films. In this figure, the PHVs and their ionization energy losses are well correlated, for the NRHRhS film. Thus, we can control the sensitivity of nuclear emulsion films by changing the amount of added Rh. On the other hand, difference of PHV values for each ion in NRHRhL emulsion films is less enhanced relative to NRHRhS films. Further investigation is required to clarify this feature.

Since the peak values of PHV for each ion were well separated in the NRHRhS emulsion films, we can distinguish each ion clearly. To apply PHV measurement by desensitized films for cosmic ray experiments, the linearity of PHV and density of rhodium compound would be preferable, because we have to extrapolate it to heavier charged particles than the ones used here in heavy ion beam experiments. Unfortunately, we cannot state a functional relationship between nuclear emulsion sensitivity and the total amount of added rhodium compound. We would need to prepare more samples with different amounts of added rhodium to establish this relationship.

The shadowing effect of overlapped grains also affects the HTS analysis. We have verified dependence of incident angle to PHV values for Li, Be, B and C ions. Grain-overlapping effects in PHV have been observed for B, Be and Li ions at the incident angle of 20°. At the incident angle of 40°, the PHVs of Be, B and C ions increased from these values at 20°. In the image analysis, HTS is applied to image filtering to eliminate noise and to reconstruct off-focus grains. Further details of HTS image processing can be found in Section 3.5 of the paper by Yoshimoto et al.[2] These image analysis processes are complicated in simulating the observed PHVs. Therefore, we must analyze the correlation between PHV and incident angles for heavier charged particles.

It is indispensable to combine solid-state detector such as CR-39 and nuclear emulsion films, because previous nuclear emulsion films with high sensitivity could not distinguish high energy particles each other. Whereas desensitized films can measure ions of Li, Be, B and C by adjusting the sensitization level of films properly, and measured results were well-consistent with the ones with CR-39. Therefore, we need not to use the hybrid system of films and CR-39 by the use of films desensitized properly.

6. Conclusion

To assess the sensitivities of nuclear emulsion films with or without the addition of rhodium compound evaluated by the PHV signals that indicate the ionization energy losses of a heavy ion beam, we exposed samples of nuclear emulsion films to 350 MeV-per-nucleon heavy ions at the HIMAC facility. We prepared five nuclear emulsion films with different sensitivity. The sensitivity of NRHRhS was decreased by 37% relative to that of RM and that of NRHRhL was decreased 54% relative to that of NRHRhS.

In the RM and NRHRhS films, we successfully obtained PHV distributions for the Li, Be, B and C beams. On the other hand, Li ions left no tracks in the NRHRhL films. In the RM film, we did not obtain any linear relationship between PHV and ionization energy losses calculated from the Bete-Bloch formula for Li, Be, B, C beams. In case of the NRHRhS and NRHRhL films, the PHV values are well correlated with the energy losses calculated from the Bete-Bloch formula. The incident-angle dependency of PHV was also examined and complex relationships were found. Finally, we confirmed the validity of the PHV signal measurement with desensitized NRHRhS and NRHRhL films to detect high-energy particles. We will not need the hybrid system with films and solid-state track-detectors such as CR-39.

We will be able to use the HTS in the F-lab. of Nagoya University for the exploration of long-duration balloon flights of the GRAINE experiment to analyze the chemical composition of galactic cosmic-ray nuclei.

Acknowledgment

This work was supported in part by the joint research program of the Institute of Materials and Systems for Sustainability, Nagoya University. We wish to acknowledge valuable discussions and advises regarding the production and scanning of nuclear emulsion films with the member of GRAINE experiments in the fundamental particle laboratory at Nagoya University. The authors would also like to thank Mr. K. Kuwabara, visiting researcher in the fundamental particle physics laboratory and Designated Prof. K. Ohzeki, Institute of Materials and Systems for Sustainability at Nagoya University, for preparing chemical compounds for desensitizing nuclear emulsion films used in this work.

References

1) K. Ozaki, S. Aoki, K. Kamada, T. Kosaka, F. Mizutani, E. Shibayama, S. Takahashi, Y. Tateishi, S. Tawa, K. Yamada, H. Kawahara, N. Otsuka, H. Rokujo, J. Instrum., **10**, P12018 (2015).
2) M. Yoshimoto, T. Nakano, R. Komatani, Hiroaki Kawahara., Prog. Theor. Exp. Phys. **2017**, 103H01 (2017).
3) Y. Nakamura, GRAINE collaboration, Balloon Symposium: 2018 (sas18-sbs-011), Institute of Space and Astronautical Science, Japan Aerospace Exploration Agency (JAXA)(ISAS), Sagamihara, Kanagawa Japan (November 1-2, 2018)(in Japanese).
4) R. Acquafredda, T. Adam, N. Agafonova, P. Alvarez Sanchez, M. Ambrosio, A. Anokhina, S. Aoki, A. Ariga, T. Ariga, L. Arrabito, C. Aufranc, D. Autiero, A. Badertscher, A. Bagulya, E. Baussan, A. Bergnoli, F. Bersani Greggio, A. Bertolin, M. Besnier, D. Biare, D. Bick, S. Blin, K. Borer, J. Boucrot, D. Boutigny, V. Boyarkin, C. Bozza, T. Brugiere, R. Brugnera, G. Brunetti, S. Buontempo, J.E. Campagne, B. Carlus, E. Carrara, A. Cazes, L. Chaussard, M. Chernyavsky, V. Chiarella, N. Chon-Sen, A. Chukanov, R. Ciesielski, L. Consiglio, M. Cozzi, G. D'Amato, F. Dal Corso, N. D'Ambrosio, J. Damet, C. de La Taille, G. De Lellis, Y. Declais, T. Descombes, M. De Serio, F. Di Capua, D. Di Ferdinando, A. Di Giovanni, N. Di Marco, C. Di Troia, N. Dick, S. Dmitrievski, A. Dominjon, M. Dracos, D. Duchesneau, B. Dulach, S. Dusini, J. Ebert, I. Efthymiopoulos, O. Egorov, K. Elsener, R. Enikeev, A. Ereditato, L.S. Esposito, C. Fanin, J. Favier, G. Felici, T. Ferber, R. Fini, L. Fournier, A. Franceschi, D. Frekers, T. Fukuda, C. Fukushima, V.I. Galkin, V.A. Galkin, R. Gallet, S. Gardien, A. Garfagnini, G. Gaudiot, G. Giacomelli, M. Giorgini, C. Girerd, C. Gollnitz, T. Goeltzenlichter, J. Goldberg, D. Golubkov, Y. Gornushkin, J.N. Grapton, G. Grella, F. Grianti, E. Gschwendtner, C. Guerin, M. Guler, C. Gustavino, J.L. Guyonnet, C. Hagner, T. Hamane, T. Hara, M. Hauger, M. Hess, M. Hierholzer, K. Hoshino, M. Ieva, M. Incurvati, K. Jakovcic, J. Janicsko Csathy, B. Janutta, C. Jollet, F. Juget, M. Kazuyama, S.H. Kim, N. Khovansky, M. Kimura, B. Klicek, J. Knusel, K. Kodama, D. Kolev, M. Komatsu, U. Kose, A. Krasnoperov, I. Kreslo, Z. Krumstein, V.V. Kutsenov, V.A. Kuznetsov, I. Laktineh, M. Lavy, C. Lazzaro, T.D. Le, T. Le Flour, J. Lenkeit, J. Lewis, S. Lieunard, A. Ljubicic, A. Longhin, G. Lutter, A. Malgin, K. Manai, G. Mandrioli, A. Marotta, J. Marteau, G. Martin-Chassard, V. Matveev, N. Mauri, M. Meddahi, F. Meisel, A. Meregaglia, A. Meschini, M. Messina, P. Migliozzi, P. Monacelli, I. Monteiro, F. Moreau, K. Morishima, U. Moser, M.T. Muciaccia, P. Mugnier, N. Naganawa, M. Nakamura, T. Nakano, T. Napolitano, V. Nikitina, K. Niwa, Y. Nonoyama, A. Nozdrin, S. Ogawa, A. Olchevski, D. Orlandi, G. Orlova, V. Osedlo, D. Ossetski, M. Paniccia, A. Paoloni, B.D. Park, I.G. Park, A. Pastore, L. Patrizii, L. Pellegrino, E. Pennacchio, H. Pessard, V. Pilipenko, C. Pistillo, N. Polukhina, M. Pozzato, K. Pretzl, P. Publichenko, F. Pupilli, L. Raux, J.P. Repellin, R. Rescigno, D. Rizhikov, T. Roganova, G. Romano, G. Rosa, I. Rostovtseva, A. Rubbia, A. Russo, V. Ryasny, O. Ryazhskaya, A. Sadovski, C. Sanelli, O. Sato, Y. Sato, V. Saveliev, G. Sazhina, A. Schembri, W. Schmidt-Parzefall, H. Schroeder, H.U. Schutz, J. Schuler, L. Scotto Lavina, J. Serrano, H. Shibuya, S. Simone, M. Sioli, C. Sirignano, G. Sirri, J.S. Song, M. Spinetti, L. Stanco, N. Starkov, M. Stipcevic, T. Strauss, P. Strolin, V. Sugonyaev, S. Takahashi, V. Talochkin, M. Tenti, V. Tereschenko, Francesco Terranova, I. Tezuka, V. Tioukov, P. Tolun, V. Tsarev, R. Tsenov, S. Tufanli, U. Ugolino, N. Ushida, G. Van Beek, V. Verguilov, T. Viant, P. Vilain, M. Vladimirov, L. Votano, J.L. Vuilleumier, T. Walchli, M. Weber, G. Wilquet, B. Wonsak, J. Wurtz, V. Yakushev, C.S. Yoon, Y. Zaitsev, A. Zghiche, R. Zimmermann, J. Instrum., **4**, P04018 (2009).
5) T. Fukuda, Proceedings of Science, The 3rd KMI International Symposium (012), **294**, Nagoya University, Nagoya Japan (January 5-7, 2017).
6) S. Takahashi, S. Aoki, K. Hamada, T. Hara, T. Inoue, K. Ishiguro, A. Iyono, H. Kawahara, K. Kodama, R. Komatani, M. Komatsu, T. Kosaka, M. Miyanishi, F. Mizutani, K. Morishima, M. Morishita, N. Naganawa, M. Nakamura, T. Nakano, A. Nishio, K. Niwa, N. Otsuka, K. Ozaki, H. Rokujo, O. Sato, E. Shibayama, A. Suzuki, R. Tanaka, Y. Tateishi, S.i Tawa, M. Yabu, K. Yamada, S. Yamamoto, M. Yoshimoto, Adv. Space Res., **62**, 2945-2953 (2018).
7) S. Takahashi, S. Aoki, K. Hamada, T. Hara, T. Inoue, K. Ishiguro, A. Iyono, H. Kawahara, K. Kodama, R. Komatani, M. Komatsu, T. Kosaka, M. Miyanishi, F. Mizutani, K. Morishima, M. Morishita, N. Naganawa, M. Nakamura, T. Nakano, A. Nishio, K. Niwa, N. Otsuka, K. Ozaki, H. Rokujo, O. Sato, E. Shibayama, A. Suzuki, R. Tanaka, Y. Tateishi, S. Tawa, M. Yabu, K. Yamada, S. Yamamoto, M. Yoshimoto, Prog. Theor. Exp. Phys., **2016**, 073F01 (2016).
8) K. Morishima, M. Kuno, A. Nishio, N. Kitagawa, Y. Manabe, M. Moto, F. Takasaki, H. Fujii, K. Satoh, H. Kodama, K. Hayashi, S. Odaka, S. Procureur, D. Attié, S. Bouteille, D. Calvet, C. Filosa, P. Magnier, I. Mandjavidze, M. Riallot, B. Marini, P. Gable, Y. Date, M. Sugiura, Y. Elshayeb, T. Elnady, M. Ezzy, E. Guerriero, V. Steiger, N. Serikoff, J. Mouret, B. Charlès, H. Helal, M. Tayoubi, Nature, **552**, 386-390, (2017).
9) D. M. Siegel, B. D. Metzger, Phys. Rev. Lett., **119**, 231102-1 - 231102-7 (2017).
10) K. Kuge, K. Yabe, N. Aoki, A. Hasegawa, N. Mii, T. Habu, J. Soc. Photogr. Sci. Tech. Jpn., **63**, 63-67 (2000)(in Japanese).
11) C. F. Powell, P. H. Fowler, D. H. Perkins, "The Study of Elementary Particles by the Photographic Method", PERGAMON PRESS, 100-112 (1959).
12) K. Kuwabara, S. Nishiyama, FUJIFILM Research & Development, **48**, 82-86 (2003).
13) N. Yasuda, S. Kodaira, M. Kurano, H. Kawashima, H. Tawara, T. Doke, K. Ogura, N. Hasebe, J. Phys. Soc. Jpn., **78**, 142-145 (2009).
14) W. R. Leo, "Techniques for Nuclear and Particle Physics Experiments", Second Revised Edition, Springer-Verlag, 24-27 (1994)
15) A. Iyono, S. Aoki, T. Hara, K. Kuretsubo, H. Matsumoto, F. Mizutani, K. Ozaki, E. Shibayama, A. Suzuki, S. Takahashi, Y. Tateishi, M. Yabu, K. Yamada, K. Kodama, K. Hamada, H. Kawahara, R. Komatani, M. Komatsu, M. Miyashita, M. Morishita, K. Morishima, M. Nakamura, N. Naganawa, T. Nakano, A. Nishio, K. Niwa, N. Otsuka, H. Rokujo, O. Sato, M. Yoshimoto, S. Yamamoto, Proceedings of Science, 35th International Cosmic Ray Conference (171), **301**, 171, Busan Korea (July 12-20, 2017).
16) K. Kuge, K. Hayashi, Y. Endo, N. Yasuda, C. Fukushima, M. Kimura, H. Shibuya, A. Hasegawa, H. Kumagai, S. Kodaira, S. Ota, J. Soc. Photogr. Sci. Tech. Jpn., **72**, 209-213 (2009).